Bubble growth by injection of gas into viscous liquids in cylindrical and conical tubes

A. López-Villa,[1] A. Medina,[2] and F. J. Higuera[3]
[1]*Coordinación del Posgrado, IMP, Eje Central Lázaro Cárdenas No. 152, Col. Atepehuacan 07730, México D.F., Mexico*
[2]*ESIME Azcapotzalco, IPN, Ave. de las Granjas No. 682, Col. Sta. Catarina 02550, México D.F., México*
[3]*ETSI Aeronáuticos, UPM, Plaza Cardenal Cisneros 3, Madrid 28040, Spain*

(Received 7 October 2010; accepted 1 September 2011; published online 14 October 2011)

The effect of partial confinement on the shape and volume of bubbles generated by injection of a constant flow rate of gas into a very viscous liquid is studied numerically and experimentally. Numerical solutions of the Stokes equations for the liquid and the evolution equation for the surface of a bubble, and experiments with two different liquids, show that cylindrical and conical walls concentric with a gas injection orifice in the horizontal bottom of the liquid may strongly affect the shape and volume of the bubbles, and can be used to control the size of the generated bubbles without changing the flow rate of gas. A well-known scaling law for the volume of the bubbles generated by injection of a high flow rate of gas in a very viscous unconfined liquid is extended to take into account the presence of cylindrical or conical walls around the injection orifice. © *2011 American Institute of Physics*. [doi:10.1063/1.3643248]

I. INTRODUCTION

The growth and detachment of bubbles generated by the continuous injection of gas into a quiescent liquid has been very much studied in conditions where the viscosity of the liquid plays no important role.[1–8] Results of these studies are of interest in metallurgical and chemical industries, for example, where liquids of low viscosity, such as liquid metals and aqueous solutions, need to be handled. Bubbles in these liquids can be used to modify the concentrations of different substances and promote chemical reactions between them, to clean liquids from impurities captured by adhesion or diffusion processes, and for many other purposes.[2]

The generation and dynamics of bubbles in very viscous liquids is also of interest but has not been so much studied. Thus, while many aspects of the dynamics of bubbles in unbounded viscous liquids are well understood,[9–14] the formation and detachment of bubbles in confined systems has received less attention.[15–18] Bubbles in very viscous liquids are commonly found when dealing with polymers in their liquid phases, in the flows of lava, and in processes of oil extraction from production pipelines, among others. The last cited example has motivated the present work, which sprang from interest in the so-called gas lift technique of enhanced oil recovery,[19] where bubbles formed by injecting gas in oil extraction pipes help pumping the oil.

Scaling laws[13–15] show that the volume of the bubbles generated by injecting a high flow rate of gas into a very viscous liquid increases as the power 3/4 of the flow rate and is independent of the diameter of the injection orifice. The simplest way to control the size of the bubbles in a given liquid is, therefore, to act on the flow rate of gas. This possibility, however, is limited in the application at hand, because the flow rate of gas to be injected in the confined space of an extraction pipe is often determined by other requirements of the gas lift technique. The limitation poses a problem to control the size of the bubbles and brings to the front elements of the generation process such as the viscous drag of the bubbles[13] and the shear stress in the vicinity of the walls,[15,17,18] which are disregarded in inviscid analyses but offer a clue to the solution of the size-control problem.

In this paper, we show that the shape of the tube in the vicinity of the injection orifice, or the use of properly shaped injection nozzles, may cause substantial distortion of the growing bubbles and modify their volume at detachment. In our analysis, a constant flow rate of gas is injected through a circular orifice in the horizontal base a container filled with a very viscous liquid, and the space where the bubbles grow is partially confined by surrounding the orifice with a vertical cylindrical wall or an inverted vertical cone. The extent of the confinement can be gradually increased by decreasing the radius of the cylinder or the angle of the cone, which allows to quantify the effect of the wall on the evolution and size of the bubbles. This size is determined numerically and experimentally, and scaling laws that are extensions of well-known laws for unconfined liquids are proposed and validated.

II. EQUATIONS FOR BUBBLES GROWING IN A CONFINED LIQUID

A constant flow rate Q of an incompressible gas of negligible density and viscosity is injected into a liquid of density ρ and viscosity μ initially at rest in a vertical tube under the action of the gravity. The gas is injected through a circular orifice of radius a at the center of the base, of radius R^*, of the tube. The lateral wall of the tube may be cylindrical or conical, making an angle α to the vertical, as sketched in Fig. 1. The height of the tube is H^* and its upper end is open to an infinite expanse of the same liquid, as sketched in the upper part of Fig. 1(a) for a cylindrical tube.

The gas accumulates in a bubble attached to the base of the tube. The volume of this bubble increases with time until

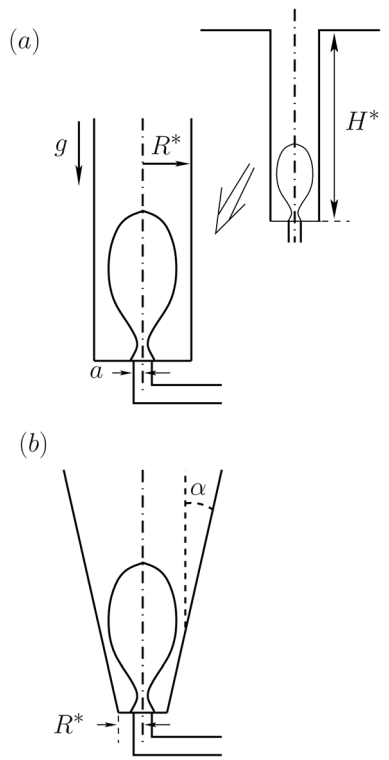

FIG. 1. Schematic of a bubble attached to the base of a cylindrical (*a*) or a conical (*b*) tube filled with a very viscous liquid.

it detaches and begins to ascend in the liquid, being replaced by a new attached bubble. The effect of the inertia is assumed to be negligible in the motion induced in the liquid by the growth and displacement of the bubbles. A sufficient condition for the effect of the inertia of the liquid to be negligible is that $Re = \rho Q/\mu R_b \ll 1$, where R_b is the characteristic radius of the detaching bubble or of its upper cap, which is to be determined (see Refs. 13, 14, and 18 and Sec. IV below).

Let $f(\boldsymbol{x},t) = 0$ be the equation of the surface of the bubble attached to the base of the tube, with $f > 0$ in the liquid. The surface of the bubble is assumed to be axisymmetric and $\boldsymbol{x} = (x,r)$, where x is the vertical distance measured upward from the base of the tube and r is the distance to its symmetry axis. Scaling distances with a and times with the viscous capillary time $\mu a/\sigma$, where σ is the surface tension of the liquid, the equations governing the evolution of the liquid and the surface of the bubble are

$$\nabla \cdot \boldsymbol{v} = 0, \tag{1}$$

$$0 = -\nabla p + \nabla^2 \boldsymbol{v} - B\,\boldsymbol{i} \tag{2}$$

in the liquid, $f(\boldsymbol{x},t) > 0$,

$$\frac{Df}{Dt} = 0, \tag{3}$$

$$-p\boldsymbol{n} + \tau' \cdot \boldsymbol{n} = (\nabla \cdot \boldsymbol{n} - p_g)\,\boldsymbol{n} \tag{4}$$

at the surface of the bubble, $f(\boldsymbol{x},t) = 0$,

$$\boldsymbol{v} = 0 \tag{5}$$

at the solid surfaces bounding the liquid, and

$$\nabla(p + B\,x) = 0 \tag{6}$$

in the upper expanse of liquid far above the tube.

Here, $p_g(t)$ is the uniform pressure of the gas in the bubble, which is to be found using the condition that the volume V of the bubble increases linearly with time at a rate equal to Q. In dimensionless variables,

$$\frac{dV}{dt} = Ca. \tag{7}$$

The contact line of the bubble with the base of the tube is a circle whose radius is determined by the condition that the angle between the surface of the bubble and the base be equal to the contact angle of the liquid with the base θ, which is assumed to be a constant.

Problem (1)–(7) contains the six dimensionless parameters

$$B = \frac{\rho g a^2}{\sigma}, \quad Ca = \frac{\mu Q}{\sigma a^2}, \quad R = \frac{R^*}{a}, \quad H = \frac{H^*}{a}, \quad \theta, \quad \alpha, \tag{8}$$

which are a Bond number, a capillary number, the dimensionless radius of the base and height of the tube, the contact angle of the liquid with the base, and the semi-angle of the conical tube.

In these equations, $\boldsymbol{i}$ is a unit vector pointing upward; $D/Dt = \partial/\partial t + \boldsymbol{v} \cdot \nabla$ is the material derivative at points of the surface of the bubble; $\boldsymbol{n} = \nabla f/|\nabla f|$ is a unit vector normal to the surface of the bubble; and $\tau' = \nabla \boldsymbol{v} + (\nabla \boldsymbol{v})^T$ is the dimensionless viscous stress tensor.

In what follows H is given a large value ($H = 100$ in the computations discussed below) to ensure that this parameter has no effect on the growth and detachment of the bubble. Numerical tests show that the only effect of increasing H further is to increase the pressure of the gas and the liquid around the bubble (p_g and p) by a constant amount proportional to H.

III. NUMERICAL METHODS

A boundary elements method is used to solve the Stokes equations (1) and (2) with the boundary conditions (4)–(6) and a second order Runge-Kutta method is used to calculate the evolution of free surface f given by Eq. (3).

Let us assume first, for simplicity, that the contact line is pinned to the edge of the orifice at the base of the tube. The case of a moving contact line is discussed below. The boundary integral equations for axisymmetric Stokes flow can be found in Refs. 20 and 21. Elements of Pozrikidis' BEMLIB library[21] have been used. In the present problem, the liquid is bounded by the surface of the bubble, which is a material surface, the solid surfaces of the tube and the bottom of the upper expanse of liquid, and a surface at infinity in this upper expanse. The velocity and stress tensor decrease in the upper expanse as the inverse of the square and the inverse of the cube of the distance to the tube, respectively (see, e.g., Ref. 22), which makes the integrals over the surface at infinity null. At any instant of time, the stress at the surface of the

bubble is known up to the constant p_g in Eq. (4), whose computation is described below, and the velocity is known at the solid surfaces. The integral equations can, therefore, be solved to compute the velocity of the liquid at the surface of the bubble and the stress at the solid surface. The surface of the bubble can then be advanced a time step, and the unknown p_g is determined to satisfy Eq. (7).

The contour of the bubble is discretized with a finite number of nodes which move as material particles. The contour of the solid surfaces is discretized with a finite number of nonuniformly spaced fixed nodes. The spacing of the nodes at the bottom of the upper expanse increases algebraically as $r \to \infty$. The nodes at the surface of the bubble are redistributed at each time step to keep them suitably spaced. Six point Gaussian quadrature with cubic spline interpolation for the known functions and linear interpolation for the unknown functions are used to evaluate the integrals between adjacent nodes. Numerical tests showed that a discretization with 120 nodes on the contour of the bubble gives sufficient resolution.

During the evolution of the bubble, the contact line coincides with the edge of the orifice if the angle of the bubble surface (computed as explained above) to the base of the tube is larger than the contact angle of the liquid; i.e., when $-\boldsymbol{i} \cdot \boldsymbol{n} < \cos\,\theta$. The contact line drifts away from the orifice when this condition ceases to be satisfied. The radius of the contact line, $r_c(t) > 1$, is then an additional unknown which is determined by imposing the additional condition $-\boldsymbol{i} \cdot \boldsymbol{n} = \cos\,\theta$ at the node of the bubble surface located at the base of the tube ($x = 0$ and $r = r_c$). This condition is similar to that used in Ref. 23 when the advancing and receding contact angles are equal to each other, and it is also similar to the first method described in Ref. 24. It is imposed by extrapolation from the nodes of the bubble surface near the contact line; see Refs. 8 and 14 for details. The value $\theta = 45°$ has been used for the contact angle in the computations discussed below. Numerical computations with other values of θ show that the effects of the contact angle and the drift of the contact line on the final volume of the bubbles are small insofar as θ is smaller than about 90°.

If the no-slip condition is strictly imposed at the base of the tube, then the pressure and viscous stresses in the liquid around the moving contact line come out inversely proportional to the distance to this line, leading to an infinite force which would prevent any motion of the contact line.[25,26] Therefore, a certain slip is necessary in a macroscopic description of a flow with a moving contact line in order to limit the divergence of the stresses. Our numerical method, as any other method, introduces slip in a region around the contact line with an effective (numerical) slip length of the order of the distance between adjacent nodes, and our solution is not grid-independent in this region. Grid-independence can be achieved in principle by introducing a explicit (physical) slip boundary condition (for example, the Navier slip condition $v_r = \ell_s \partial v_r/\partial x$ at $x = 0$ and $r > r_c$, where v_r is the radial component of the velocity and ℓ_s is a slip length) and using a node spacing small compared to ℓ_s. However, this latter condition is difficult to fulfill in a macroscopic computation, because microscopic models suggest that the slip length should scale with the intermolecular distance.[23,26] Fortunately, many results in the literature (e.g., Moriarty and Schwartz[27]), and our numerical tests for the problem at hand, show that there is no discernible difference between a solution obtained with numerical slip and one obtained with a physical slip condition but a node spacing large compared to the slip length ℓ_s. This result is in line with the weak, logarithmic dependence of the force on the slip length to be expected for stresses that vary inversely with $(r - r_c)$ for $(r - r_c) \gg \ell_s$. It allows computing reasonable solutions of our problem without having to resort to the extremely fine grids that would be needed to resolve the microscopic slip length.

The computation stops when the radius of the neck that develops during the evolution of the bubble becomes smaller than a certain cutoff value which is of the order of the local spacing of the material nodes. This cutoff was set to 0.05, though numerical tests show that the results are not very sensitive to this value. Upon reaching the cutoff, the time to detachment is computed by linearly extrapolating the radius of the neck to zero (see Ref. 32 and Sec. IV A below). The volume of gas above the neck, augmented by the small volume injected between the end of the computation and the extrapolated detachment time, is assigned to the detaching bubble, and the rest of the volume is assigned to the new bubble that grows at the base of the tube. The surface is smoothed and reconnected using the cubic splines that are used for interpolation in the rest of the computation.

The numerical results discussed below were obtaining allowing two or three cycles of bubble growth and detachment before storing any data, in order to minimize the effect of the initial state of the liquid ($\boldsymbol{v} = 0$).

IV. RESULTS AND DISCUSSION

A. Cylindrical tubes ($\alpha = 0$)

1. Order of magnitude estimates

In this section, we revert partially to dimensional variables, which are denoted by asterisks. Thus, V_f^* will denote the volume of a bubble at the instant of detachment while $V_f = V_f^*/a^3$ is its dimensionless counterpart. For reference, consider first the much-studied case of an infinite reservoir ($R \to \infty$), in which two extreme regimes of simple bubbling have been identified; see Refs. 4 and 15. The first of these is a quasi-hydrostatic regime realized for small flow rates, when the forces on the surface of the attached bubble due to the motion of the liquid are small compared to the hydrostatic pressure and surface tension forces. In this regime, the balance of the buoyancy force pushing the bubble upward and the restraining surface tension force that acts across the contact line reads $\rho g V_f^* \sim \sigma a$ when the radius of the contact line is of the order of a. This balance gives $V_f \sim 1/B$. The second regime is a dynamic, high flow rate regime in which the restraining effect of the surface tension is negligible and the relevant balance of forces on the bubble is $\rho g V_f^* \sim \tau^* V_f^{*2/3}$, where $\tau^* \sim \mu v^*/V_f^{*1/3}$ with $v^* \sim Q/V_f^{*2/3}$ is the order of the flow-induced pressure and viscous stresses. This balance gives $V_f \sim (Ca/B)^{3/4}$. The transition between the two regimes occurs for $Ca = O(1/B^{1/3})$. If $B \ll 1$, then the attached

bubble is nearly spherical in the first regime and in the range of capillary numbers $1/B^{1/3} \ll Ca \ll 1/B$ in the second regime.

The wall of the tube begins to affect these results when R is not large compared to $V_f^{1/3}$, and the effect becomes dominant when $R \ll V_f^{1/3}$. In the quasi-hydrostatic regime, this condition amounts to $B^{1/3}R \ll 1$ and leads to a spherical cap advancing through the tube. The velocity induced in the liquid above the cap by the injection of gas is $v^* \sim Q/R^{*2}$, and the flow-induced pressure and viscous stresses on the cap are $\tau^* \sim \mu v^*/R^*$. These stresses become of the order of the surface tension stress when the capillary number based on the radius of the tube, $Ca_R = Ca/R^2$, becomes of $O(1)$, which marks the end of the quasi-hydrostatic regime. Since the Bond number based on the radius of the tube, $B_R = BR^2$, is small in the regimes described in this paragraph, the buoyancy force has no important effect on the flow around the cap and these regimes are of limited interest for bubble generation. The limiting problem coincides with the problem of a gas slug moving slowly through a liquid-filled horizontal tube, in which the advancing cap leaves behind a liquid film whose thickness is small compared to the radius of the tube when $Ca_R \ll 1$ (Refs. 28–30) and tends to a limiting value of the order of the radius of the tube when Ca_R increases.[29–31]

In the high-flow-rate regime, the condition $R \ll V_f^{1/3}$ leads to a columnar bubble with a radius of the order of the radius of the tube and a height at detachment $L_f \gg R$. In these conditions, $V_f \sim R^2 L_f$ and the estimates for an infinite reservoir need modification. The estimate of the flow-induced stresses on the cap is still valid, and the relevant balance of forces on a columnar bubble is $\rho g R^{*2} L_f^* \sim \tau^* R^{*2}$, which gives $L_f/R \sim Ca/(BR^4)$, or $V_f \sim Ca/(BR)$. If $B^{1/3}R$ is not small, then the effect of the finite radius of the tube comes into play already in the high-flow-rate regime when Ca becomes of order BR^4, and the cap of the bubble can be nearly spherical if $BR^4 \ll Ca \ll R^2$.

2. Numerical results

Some numerical computations have been carried out to study the growth and detachment of a bubble in a cylindrical tube and to validate the estimations above. Figure 2 shows a bubble which is about to detach from the base of the tube for $B = 0.2$, $Ca = 10$, and the three values $R = 5$, 4, and 3.5 of the dimensionless radius of the tube. Figure 3 shows the values at detachment of the bubble volume V_f and aspect ratio Γ (defined as the ratio of L_f to the maximum diameter of the bubble) as functions of R. The finite radius of the reservoir affects only the high-flow-rate regime for the values of B and R used here. The decrease of Γ with increasing R in Fig. 3(b) is in qualitative agreement with the estimate $L_f/R \sim Ca/(BR^4)$ for columnar bubbles. The decrease of V_f in Fig. 3(a) also agrees with the previous estimates, according to which the ratio of the volume of a columnar bubble to the volume of a bubble detaching in an infinite reservoir is of order $(Ca/B)^{1/4}/R$ for Ca/B large compared to R^4.

Figure 4 shows V_f as a function of Ca for $B = 0.2$ and three values of R. The nearly linear increase of V_f agrees with the estimate $V_f \sim Ca/(BR)$. Notice, for comparison, that

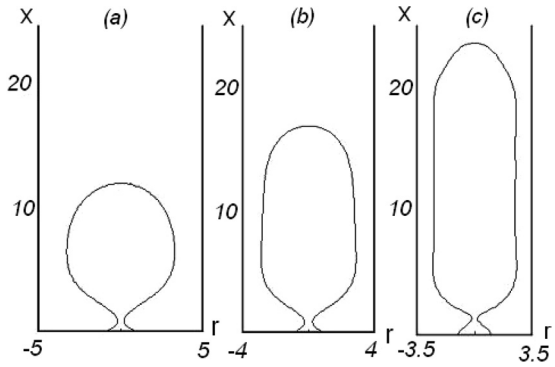

FIG. 2. Meridional section of a bubble which is about to detach from the base of a cylindrical tube for $B = 0.2$, $Ca = 10$, and $R = 5$ (*a*), 4 (*b*), and 3.5 (*c*).

$V_f \sim (Ca/B)^{3/4}$ for a bubble in an infinite reservoir. The numerical computations also show (results not displayed) that the center of mass of a columnar attached bubble rises linearly with time during the growth of the bubble, and that the velocity of the center of mass is nearly constant, except in the early stages of the process, when the bubble is still small compared to the radius of the tube.

Additional computations with $B = 0.1$, $R = 2.5$, and small values of Ca show a thin liquid film between the bubble and the wall, whose thickness decreases with Ca. This is in line with the results of Bretherton,[28] though here $B_R = BR^2 = 0.625$ is not small enough for the effect of the buoyancy to be negligible. The computations could not be extended to values of $Ca_R = Ca/R^2$ smaller than about 0.03, at which the liquid film seems to develop a corrugation, due to lack of resolution when the film becomes very thin. Series of computations in which Ca is increased keeping $B = 0.2$ and $R = 5$, or in which R is decreased keeping $B = 0.2$ and $Ca = 10$, show that the thickness of the liquid film scaled with R tends to a constant value of about 0.3 when Ca_R increases. This value is not far from the limiting value of

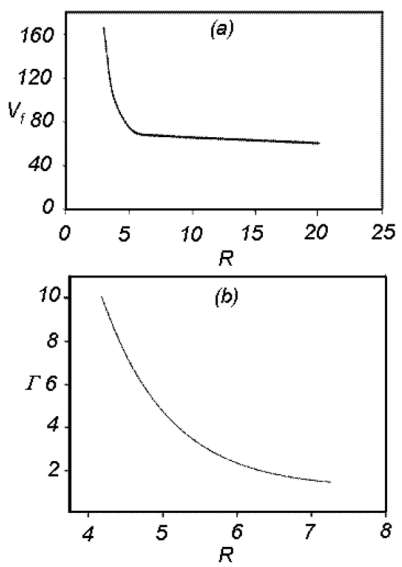

FIG. 3. (*a*) Volume V_f and (*b*) aspect ratio Γ, defined in the text, of a bubble at detachment from the base of a cylindrical tube as functions of R for $B = 0.2$ and $Ca = 10$.

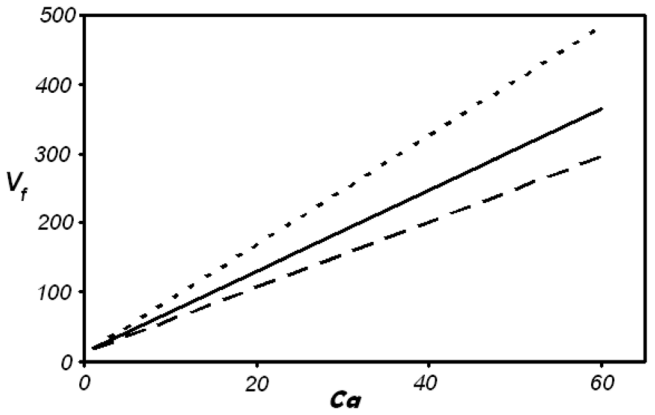

FIG. 4. Volume of a bubble at detachment from the base of a cylindrical tube as a function of Ca for $B=0.2$ and $R=4$ (dotted), 5 (solid), and 6 (dashed).

about 0.36 found by Taylor[31] (see also Martinez and Udell[30]) for a gas slug moving through a horizontal tube.

A neck forms during the evolution of the bubble and snaps at detachment. In the cases that have been computed, the final steps of this pinchoff process are not much affected by the finite radius of the tube and seem to follow the non-universal, quadratic breakup dynamics investigated by Surio *et al.*,[32] as in computations carried out elsewhere for an infinite reservoir.[14] The volume of the detached bubble is computed as described in Sec. III.

B. Conical tubes

Figure 5 shows the shape of a bubble which is about to detach from the base of a conical tube for $B=0.2$, $Ca=50$, $R=1.2$, and various values of the semi-angle of the cone, and Fig. 6 shows the volume V_f and the aspect ratio Γ of the detaching bubble as functions of α for $R=1.2$ and different couples of values of B and Ca. As can be seen, the volume of the bubble always increases when the angle of the cone decreases, the effect being more pronounced for small values of the Bond number, for which the bubble is larger and, therefore, more easily affected by the wall of the tube.

Figure 6(a) displays an important result of this work, namely that, at low Bond numbers and high capillary numbers, the volume of the bubbles can be easily controlled through the angle of the cone without having to change the flow rate. This is a desirable possibility in some applications.

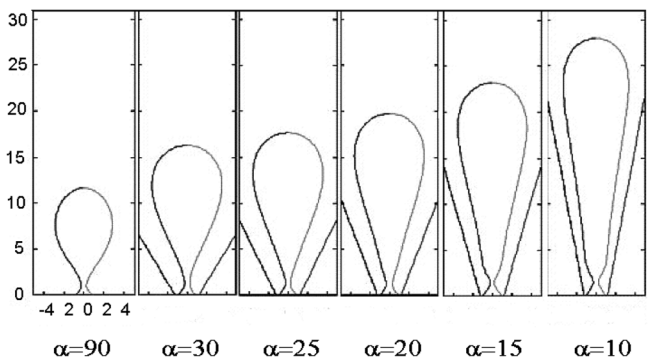

FIG. 5. Meridional section of a bubble which is about to detach from the base of a conical tube for $B=0.2$, $Ca=50$, $R=1.2$, and various values of α.

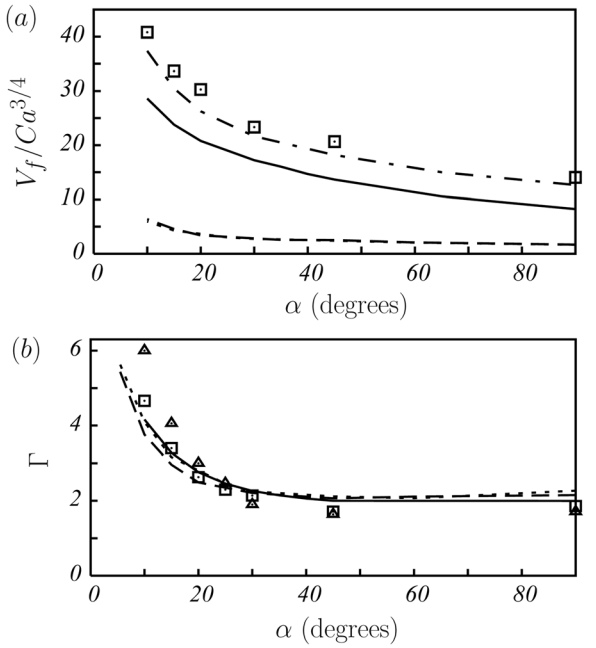

FIG. 6. (*a*) Volume V_f scaled with $Ca^{3/4}$ and (*b*) aspect ratio Γ of a bubble at detachment from the base of a conical tube as functions of α for $R=1.2$ and $(B, Ca)=(0.2, 10)$ (solid), (2, 10) (dashed), (2, 20) (dotted), and (0.15, 50) [chain, in (*a* only)]. Symbols show the values of $V_f/Ca^{3/4}$ and Γ measured experimentally for $B=0.0176$ (Δ) and $B=0.15$ (□), with $Ca=50.78$, $R=1.2$ and different values of α.

These numerical results can be rationalized by means of a straightforward extension of the estimations of Sec. IV A 1 for the high-flow-rate regime in cylindrical tubes. Figure 5 shows that the bubbles in conical tubes are columnar for moderately small values of α, with a cap that increases linearly with its height above the base of the tube. (See also Fig. 6(b); the bubble is slender for α smaller than about 30°.) Using the notation of Sec. IV A 1 and assuming that $\alpha L_f^* \gg R^*$, so that the characteristic size of the cap (αL_f^*) is large compared to the radius of the base of the tube, the characteristic velocity of the liquid around the cap is $v^* \sim Q/(\alpha L_f^*)^2$, the characteristic viscous and pressure stresses on the cap are $\tau^* \sim \mu v^*/(\alpha L_F^*)$, and the balance of buoyancy and flow-induced forces on the bubble becomes $\rho g(\alpha L_f^*)^2 L_f^* \sim \tau^* \ (\alpha L_f^*)^2$, whence $L_f \sim (Ca/B)^{1/4}/\alpha^{3/4}$ and $V_f \sim (Ca/B)^{3/4}/\alpha^{1/4}$ in dimensionless variables. This estimate coincides with the estimate for the high-flow-rate regime in an infinite reservoir[15] when $\alpha = O(1)$, and shows that the volume of the bubble increases when α decreases. The condition $\alpha L_f^* \gg R^*$ used above amounts to $Ca/B \gg R^4/\alpha$. The estimate for a cylindrical tube should be used when $Ca/B \ll R^4/\alpha$. Finally, surface tension stresses on the cap of the bubble become important when $\sigma/(\alpha L_f^*) \sim \tau^*$, which determines a lower bound capillary number, $Ca = O(\alpha/B)$, below which the estimate is not valid.

V. EXPERIMENTS

A series of experiments have been carried out to study the growth and detachment of bubbles in very viscous liquids.

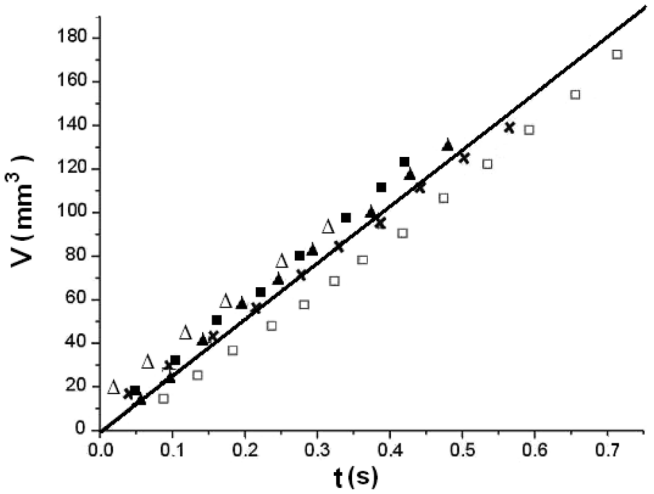

FIG. 7. Volume of a bubble attached to the base of a conical tube filled with glycerine as a function of time during the growth of the bubble for $B=0.0176$, $R=1.2$, and different values of the semi-angle of the cone. $\alpha=10°$ (□), 20° (×), 25° (▲), 30° (■), and 90° (Δ).

Glycerine and silicone oil have been used in different experiments. The properties of glycerine at 25° are: density $\rho=1260$ kg/m^3, viscosity $\mu=7.9\times10^{-1}$ N s/m^2, and surface tension $\sigma=6.3\times10^{-2}$ N/m. The properties of the silicone oil at the same temperature are: density $\rho=971$ kg/m^3, viscosity $\mu=9.71\times10^{-1}$ N s/m^2, and surface tension $\sigma=2.12\times10^{-2}$ N/m. In each experiment, a large open container with a horizontal bottom where a circular orifice of radius $a=0.3$ mm has been drilled was filled with the chosen liquid to a height of 100 mm. A glass tube of inner radius $R^*=3.2$ mm was set vertically and concentrically with the orifice to form a cylindrical tube. Conical tubes of various angles were formed by carefully inserting cones made of acetate sheet concentrically with the orifice.

Air was pumped through a capillary tube 40 cm long and 0.6 mm of inner diameter which ends at the orifice in the bottom of the container. We found in a previous work[7] that a length of 40 cm suffices to make the pressure drop in the air line large compared to the pressure variations in the bubble during the growth process and, therefore, ensure a constant flow rate in our experiments, which is one of the premises of the numerical work. To check that the flow rate is constant, the evolution of the attached bubble was video recorded; the contour of the bubble was extracted from the video images using a standard algorithm[33] implemented in a home made code; and the volume of the bubble, $V(t)$ and the height of its center of mass, $x_{CM}(t)$ were computed assuming that the bubble is axisymmetric. Some sample plots of V as a function of time for a bubble growing in glycerine within conical tubes of various angles are shown in Fig. 7. The approximately linear variation of V with time shows that the flow rate is nearly constant and independent of the angle of the cone. The value of the flow rate determined by fitting a straight line to the experimental data of Fig. 7 is $Q=364.5$ mm^3/s. The same procedure was used to measure the flow rate of air injected into silicone oil and in cylindrical tubes. The flow rate was found to be nearly constant in all the cases.

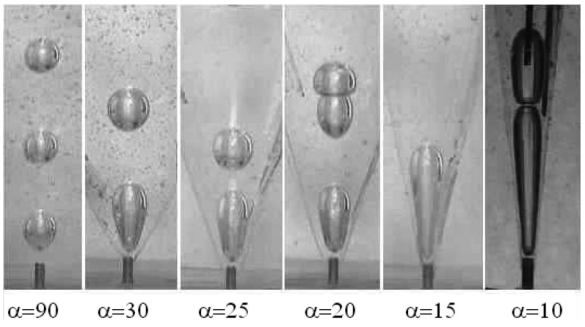

FIG. 8. Images of a bubble which is about to detach from the base of a conical tube for $B=0.0176$, $Ca=50.78$, $R=1.2$, and various values of the semi-angle of the cone.

Figure 8 shows the shapes of bubbles in glycerine which are about to detach from the injection orifice in conical tubes of various angles. Here, $\alpha=90°$ corresponds to a bubble detaching in an infinite reservoir, and the shape of the bubbles begin to differ significantly from this case when α becomes smaller than about 30°. Coalescence between previously detached bubbles can be seen in some of the images. The presence of the conical wall increases the drag of the ascending bubbles, decreasing their velocity and apparently promoting coalescence. We plan to analyze this important aspect of the generation of bubbles in a future work. The gas flow rate in this sequence of experiments is that measured from Fig. 7. Values of the dimensionless parameters are $B=0.0176$, $Ca=50.78$, and $R=1.2$.

The final volume V_f and aspect ratio Γ of the bubbles in Fig. 8 and others were extracted from the images and included in Fig. 6 (triangles and squares), where they are compared to numerical results obtained for similar values of the dimensionless parameters. The comparison is reasonably good, though the experimental values of Γ increase with decreasing α somewhat faster than the numerical values, and become larger than them for small values of α. We think that the difference is due to the vertical momentum injected with the gas, which was not taken into account in the numerical computations.

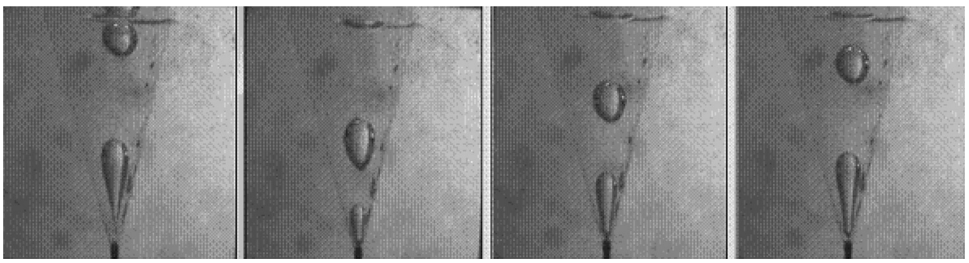

FIG. 9. Four equispaced images spanning the period of growth of a bubble attached to the base of a conical tube for $B=0.04$, $Ca=70.23$, $R=1.2$, and $\alpha=15°$. The period of bubbling is 1 s.

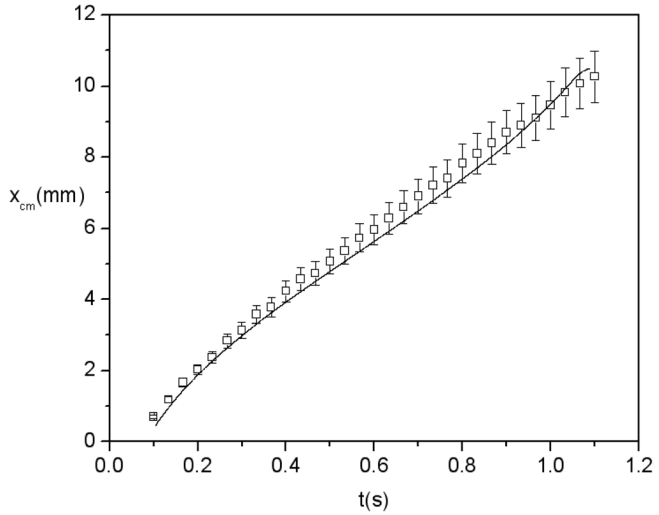

FIG. 10. Height of the center of mass of a bubble attached to the base of a conical tube as a function of time during the growth of the bubble for $B=0.04$, $Ca=70.23$, $R=1.2$, and $\alpha=15°$. Symbols are experimental results and the solid curve shows the results of the numerical computation.

Figure 9 shows four equispaced images of a bubble growing in silicone oil within a conical tube of semi-angle $\alpha=15°$. The flow rate is $Q=138$ mm^3/s, leading to $B=0.04$, $Ca=70.23$, and $R=1.2$. The period of bubbling is 1 s. The evolution of the center of mass of the bubble is shown in Fig. 10 and compared to numerical results. The nearly linear increase of x_{CM} with time is to be compared to the $x_{CM} \propto t^{1/3}$ evolution expected for a round bubble growing in an infinite reservoir.[15] The difference clearly shows the effect of the conical wall.

Only silicone oil was used in experiments with cylindrical tubes because glycerine tends to produce small bubbles that linger in the tube for a long time and interfere with the observation of the bubble attached to the orifice. Figure 11 shows five images equispaced in time that span the cycle of growth and detachment of a bubble. The flow rate of gas measured from the video record is $Q=419.59$ mm^3/s in this experiment, and the period of bubbling is 1.33 s. Values of the dimensionless parameters are $B=0.04$, $Ca=209.94$, and $R=10.66$. Figure 12 shows the position of the center of mass of the bubble as a function of time. As was to be expected from the columnar character of the bubble, x_{CM} increases linearly with time during most of the evolution, with the exception of two short intervals at the beginning and the end of the process.

VI. CONCLUSIONS

The growth of a bubble due to the injection of a constant flow rate of a gas through an orifice in the horizontal base of a tube filled with a very viscous liquid has been investigated numerically and experimentally in conditions when nearby solid walls partially confine the space where the bubble is allowed to grow. Conical and cylindrical walls coaxial with the injection orifice have been used to allow easy control of the extent of the confinement by simply changing the angle of the cone or the radius of the cylinder.

Numerical solutions of the Stokes equations for the liquid and the evolution equation for the free surface of the bubble show that the wall near the injection orifice may have an important effect on the shape of the bubble and its volume at detachment. Computations for small Bond numbers ($B=0.2$) and moderately large capillary numbers (of the order of 10) show that vertically elongated bubbles with volumes significantly larger than those of the round bubbles generated in the absence of walls are obtained when the radius of the cylindrical wall is smaller than about six times the radius of the orifice, or when the semi-angle of the cone is smaller than about 30°. The computed distributions of forces on the surface of the bubble and the wall suggest that buoyancy, viscous drag, and viscous friction with the wall all play a role in the dynamics of the bubbles. Experiments have been carried out with two different viscous liquids that have allowed to explore wide ranges of the Bond and capillary numbers keeping the effect of the inertia of the liquid small. Good qualitative agreement has been found between numerical and experimental results. The known scaling law for the volume of a bubble at detachment from the bottom of an unconfined liquid has been extended to take into account the presence of conical or cylindrical walls. For a conical tube, the semi-angle of the cone appears as an extra factor $\alpha^{-1/4}$ multiplying the standard $(Ca/B)^{3/4}$ scaling. For a

FIG. 12. Height of the center of mass of a bubble attached to the base of a cylindrical tube as a function of time during the growth of the bubble for $B=0.04$, $Ca=209.94$, and $R=10.66$.

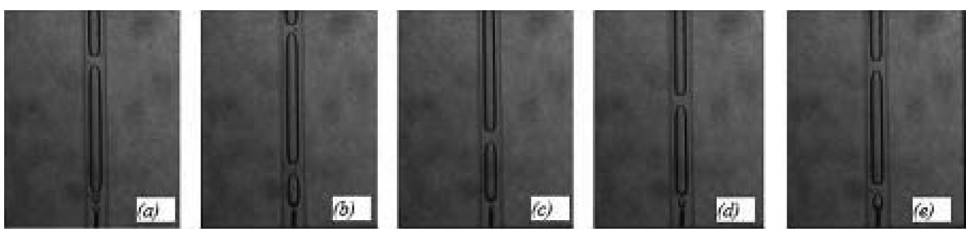

FIG. 11. Five equispaced images spanning the period of growth of a bubble attached to the base of a cylindrical tube for $B=0.04$, $Ca=209.94$, and $R=10.66$. The period of bubbling is 1.33 s.

cylindrical tube, the exponent may change from 3/4 to 1 when the radius of the cylinder decreases.

The results of the work may have a bearing on the gas lift method of enhanced oil recovery, where properly shape injection nozzles may allow optimizing the volume of the bubbles generated in oil production pipes without having to change the flow rate of gas.

ACKNOWLEDGMENTS

The authors are grateful to Professor Y. Ryazantzev (UPM, Madrid) for his suggestion to study the growth of bubbles in conical containers. The participation of A.M. in this work was funded by IPN through the SIP Project No. 201000890, and by CONACYT through an equipment grant. F.J.H. acknowledges support from the Spanish Ministerio de Ciencia e Innovación through Project No. DPI2010-20450-C03-01. Some experiments were carried out by the PIFI students A. Santana and C. Soriano, to whom the authors express their gratitude.

[1]R. Kumar and N. R. Kuloor, "The formation of bubbles and drops," Adv. Chem. Eng. **8**, 255 (1970).
[2]R. Clift, J. R. Grace, and M. E. Weber, *Bubbles, Drops, and Particles* (Academic, San Diego, 1978).
[3]N. Rabiger and A. Vogelpohl, *Bubble Formation and its Movement in Newtonian and Non-Newtonian Liquids Encyclopedia of Fluid Mechanics*, *Vol. 3*, edited by N. P. Cheremisinoff (Gulf Publishing Corporation, Houston, 1986).
[4]M. S. Longuet-Higgins, B. R. Kerman, and K. Lunde, "The release of air bubbles form and underwater nozzle," J. Fluid Mech. **230**, 365 (1991).
[5]H. N. Oguz and A. Prosperetti, "Dynamics of bubble growth and detachment from a needle," J. Fluid Mech. **257**, 111 (1993).
[6]S. S. Sadhal, P. S. Ayyaswamy, and J. N. Chung, *Transport Phenomena with Drops and Bubbles* (Springer-Verlag, Berlin, 1997).
[7]G. Corchero A. Medina, and F. J. Higuera, "Effect of wetting conditions and flow rate on bubble formation at orifices submerged in water," Colloids Surf., A **290**, 41 (2006).
[8]F. J. Higuera and A. Medina, "Injection and coalescence of bubbles in a quiescent invicid liquid," Eur. J. Mech. B/Fluids **25**, 164 (2006).
[9]R. B. Bird, R. C. Armstrong, and U. Hassager, *Dynamics of Polymeric Liquids* (Wiley-Interscience Publication, New York, 1987).
[10]D. L. Sahagian, "Bubble migration and coalescence during solidification of basaltic lava flows," J. Geol. **93**, 205 (1985).
[11]M. Manga and H. A. Stone, "Interactions between bubbles in magmas and lavas: Effects of the deformation," J. Volcanol. Geotherm. Res. **63**, 269 (1994).
[12]M. Manga, J. Castro, and K. V. Cashman, "Rheology of bubble-bearing magmas," J. Volcanol. Geotherm. Res. **87**, 15 (1998).
[13]H. Wong, D. Rumschitzki, and C. Maldarelli, "Theory and experiment on the low-Reynolds-number expansion and contraction of a bubble pinned at a submerged tube tip," J. Fluid Mech. **356**, 93 (1998).
[14]F. J. Higuera, "Injection and coalescence of bubbles in a very viscous liquid," J. Fluid Mech. **530**, 369 (2005).
[15]J. F. Davidson and B. O. G. Schuler, "Bubble formation at an orifice in a viscous liquid," Trans. Inst. Chem. Eng. **38**, 144 (1960).
[16]Q. C. Bi and T. S. Zhao, "Taylor bubbles in miniaturized circular and noncircular channels," Int. J. Multiphase Flow **27**, 561 (2001).
[17]A. M. Jacob and D. P. Graver III, "An investigation of the influence of cell topography on epithelial mechanical stresses during pulmonary airway reopening," Phys. Fluids **17**, 031502 (2005).
[18]V. S. Ajaev and G. M. Homsy, "Modeling shapes and dynamics of confined bubbles," Annu. Rev. Fluid Mech. **38**, 277 (2006).
[19]K. E. Brown, *The Technology of Artificial Lift Methods* (Penn-well Books, Oklahoma, 1977), Vol. 4.
[20]C. Pozrikidis, *Boundary Integral and Singularity Methods for Linearized Viscous Flows* (University Press, Cambridge, 1992).
[21]C. Pozrikidis, *A Practical Guide to Boundary Element Methods* (Chapman and Hall/CRC, New York, 2002).
[22]W. N. Bond, "Viscous flows through wide angled cones," Philos. Mag. **50**, 1058 (1925).
[23]Y. Chen, R. Mertz, and R. Kulenovic, "Numerical simulation of bubble formation on orifice plates with a moving contact line," Int. J. Multiphase Flow **35**, 66 (2009).
[24]M. Renardy, Y. Renardy, and J. Li, "Numerical simulation of moving contact line problems using a volume-of-fluid method," J. Comput. Phys. **171**, 243 (2001).
[25]G. K. Batchelor, *An Introduction to Fluid Dynamics* (Cambridge University Press, Cambridge, 1967).
[26]W. Ren and W. E, "Boundary conditions for the moving contact line problem," Phys. Fluids **19**, 022101 (2007).
[27]J. A. Moriarty and L. W. Schwartz, "Effective slip in numerical calculations of moving-contact-line problems," J. Eng. Math. **26**, 81 (1992).
[28]F. P. Bretherton, "The motion of long bubbles in tubes," J. Fluid Mech. **10**, 166 (1961).
[29]L. W. Schwartz, H. M. Princen, and A. D. Kiss, "On the motion of bubbles in capillary tubes," J. Fluid Mech. **172**, 259 (1986).
[30]M. J. Martinez and K. S. Udell, "Boundary integral analysis of the creeping flow of long bubbles in capillaries," J. Appl. Mech. **56**, 211 (1989).
[31]G. I. Taylor, "Deposition of a viscous fluid on the wall of a tube," J. Fluid Mech. **10**, 161 (1961).
[32]R. Surio, P. Doshi, and O. Basaran, "Non-selfsimilar, linear dynamics during pinchoff of a hollow annular jet," Phys. Fluids **16**, 4177 (2004).
[33]J. C. Russ, *The Image Processing Handbook* (CRC, Boca Raton, Florida, 2002).